of Gifu University for providing the facilities for ESR measurements and for his kind advice on a electrochemical ESR cell. We also thank Mr. Hidekazu Akamatsu for preliminary experimental work. This work was partially supported by a Grant-in-Aid from Ministry of Education, Science and Culture of Japan.

Supplementary Material Available: Figure 5 plotting the percent protonation of **12** against H_0 of the solvent (1 page). Ordering information is given on any current masthead page.

12-Crown-4 Ethers: Solid-State Stereochemical Features of Dibenzo-12-crown-4, Derived Dicyclohexano-12-crown-4 Isomers, and a Lithium Thiocyanate Complex As Determined via ^{13}C CPMAS Nuclear Magnetic Resonance and X-ray Crystallographic Methods

G. W. Buchanan* and R. A. Kirby

Ottawa-Carleton Chemistry Institute, Department of Chemistry, Carleton University, Ottawa, Canada K1S 5B6

J. P. Charland and C. I. Ratcliffe

Division of Chemistry, National Research Council of Canada, Ottawa, Canada K1A 0R9

Received June 28, 1990

Solid-phase ^{13}C NMR spectra are presented for the title systems. For dibenzo-12-crown-4, *cis-anti-cis*-dicyclohexano-12-crown-4, and the LiNCS complex of the cis-syn-cis isomer, asymmetric units derived from the NMR data are consistent with single-crystal X-ray data. In the uncomplexed cis-syn-cis isomer, intermolecular crystal packing effects are shown to render intramolecularly equivalent carbons nonequivalent. Some factors contributing to the ^{13}C steric shifts in these molecules are discussed.

Introduction

The stereochemical features of solid 12-crown-4 ether itself have been well documented, its crystallographic conformation having been elucidated by X-ray methods at a temperature of −150 °C.[1] Upon complexation with a variety of metal ions, three different ring conformations also have been determined by X-ray crystallography.[2-6] In contrast, the related dibenzo-12-crown-4 ether (**1**) has been reported to be incapable of acting as a host molecule for complexation.[7] The crystal structure of **1** has been reported,[8,9] and the results indicate a large deviation from planarity for the four oxygen atoms, which may account in part for the material's inability to form isolable complexes with metal ions.

To date, no reports of the solid-state properties of the related dicyclohexano-12-crown-4 ether systems have appeared. These molecules are expected to exhibit more stereochemical flexibility than their dibenzo precursor and hence may be capable of forming isolable complexes. Herein we present the details of the X-ray crystallographic results for the cis-anti-cis (**2**) and cis-syn-cis (**3**) isomers of dicyclohexano-12-crown-4, as well as the LiNCS complex of **3**.

In addition, we have recorded the ^{13}C CPMAS NMR spectra of **1**, **2**, **3**, and **3**·LiNCS, which further illustrate the utility of this technique[10-13] for the determination of the asymmetric units in the crystal. Some remarkably large steric ^{13}C shifts have been observed in these solids and with the X-ray data in hand, a detailed discussion of geometrical influences on carbon chemical shifts is presented.

Chart I. Comparison of Torsion Angles for C7 and C8 of 2 (H's Not Included)

C_7		C_8	
network	θ, deg	network	θ, deg
O2-*C7*-C8-O1	78.2	O_2-C7-*C8*-O1′	78.2
C7-O2-C2-C1	149.4	*C8*-O1′-C1′-C2′	99.1
C7-O2-C2-C3	90.7	*C8*-O1′-C1′-C6′	136.4
C7-C8-O1′-C1′	165.4	*C8*-C7-O2-C2	106.1
C8-*C7*-O2-C2	106.1	*C7*-C8-O1′-C1′	165.4

Results and Discussion

The structural formulae and numbering schemes for the molecules studied herein are depicted in Figure 1. The numbering schemes employed are chosen to be consistent with X-ray data output rather than with IUPAC convention. Bond lengths and angles for **2**, its configurational isomer **3**, and **3**·LiNCS are listed in Table I. Torsion angles involving ring skeletal atoms for **2**, **3**, and **3**·LiNCS are provided in Table II and Chart I along with data for 12-crown-4 itself. Figure 2 shows stereoviews of the derived crystal structures while the ^{13}C CPMAS NMR spectra are presented in Figures 3-5. In Table III are listed the solid-phase ^{13}C NMR chemical shifts for **1**, **2**, **3**, and **3**·

(1) Groth, P. *Acta Chem. Scand. A* **1979**, *32*, 279.
(2) van Remoortere, F. P.; Boer, F. P. *Inorg. Chem.* **1974**, *13*, 2071.
(3) Boer, F. P.; Neuman, M. A.; van Remoortere, M. A.; Steiner, E. C. *Inorg. Chem.* **1974**, *13*, 2826.
(4) North. P. P.; Steiner, E. C.; van Remoortere, F. P.; Boer, F. P. *Acta Crystallogr. B* **1976**, *32*, 370.
(5) van Remoortere, F. P.; Boer, F. P.; Steiner, E. C. *Acta Crystallogr. B* **1975**, *31*, 1420.
(6) Neuman, M. A.; Steiner, E. C.; van Remoortere, F P.; Boer, F. P. *Inorg. Chem.* **1975**, *14*, 734.
(7) Pedersen, C. J. *J. Am. Chem. Soc.* **1967**, *89*, 7017.
(8) Hughes, D.; Nowell, I. W. *J. Chem. Res.* **1978**, 1531.
(9) Charland, J. P.; Buchanan, G. W.; Kirby, R. A. *Acta Crytallogr.* **1989**, *45*, 165.
(10) Belton, P. S.; Tanner, S. F.; Wright, K. M.; Payne, M. P.; Truter, M. R.; Wingfield, J. N. *J. Chem. Soc., Perkin Trans. 2* **1985**, 1307.
(11) Buchanan, G. W.; Ripmeester, J. A.; Bovenkamp, J. W.; Rodrigue, A. *Tetrahedron Lett.* **1986**, *27*, 2239.
(12) Buchanan, G. W.; Khan, M. Z.; Ripmeester, J. A.; Bovenkamp, J. W.; Rodrigue, A. *Can. J. Chem.* **1987**, *65*, 2564.
(13) Buchanan, G. W.; Kirby, R. A.; Charland, J. P. *J. Am. Chem. Soc.* **1988**, *110*, 2477.

0022-3263/91/1956-0203$02.50/0

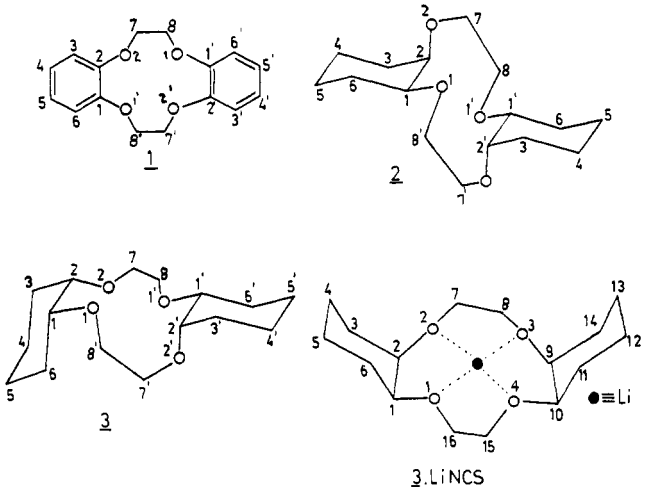

Figure 1. Structures and numbering schemes.

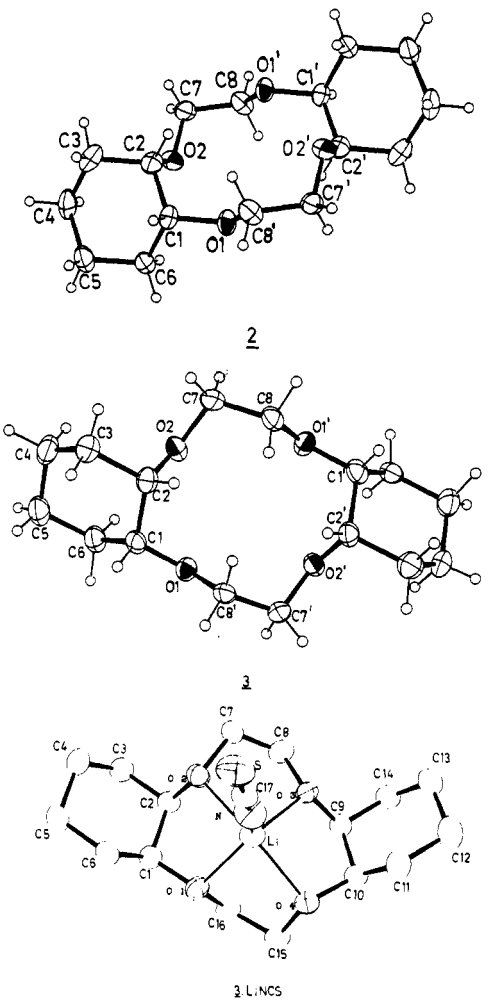

Figure 2. ORTEP diagrams for 2, 3, and 3·LiNCS.

LiNCS as well as the solution ^{13}C shifts at 298 K.

(i) Dibenzo-12-crown-4 (1). The ^{13}C NMR spectrum of 1 in solution exhibits four resonances indicating rapid stereochemical averaging between conformers of the 12-membered ring on the NMR time scale. This observation is consistent with that found for 12-crown-4 itself[14,15] where conformational interconversions become slow on the NMR time scale only at temperatures near 160 K.

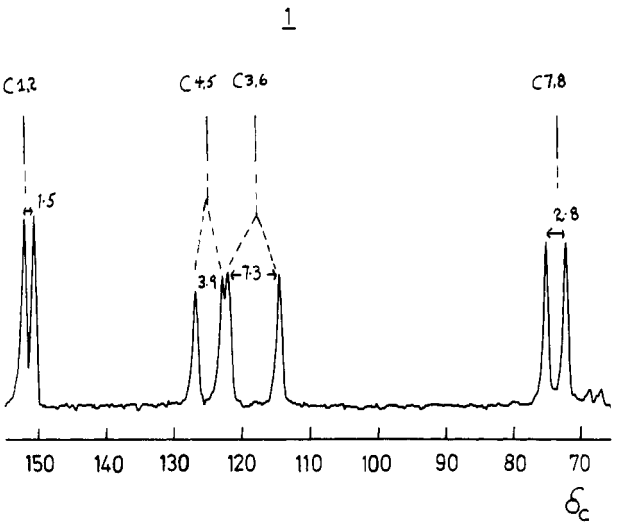

Figure 3. 45.3-MHz solid-phase ^{13}C NMR spectrum of 1.

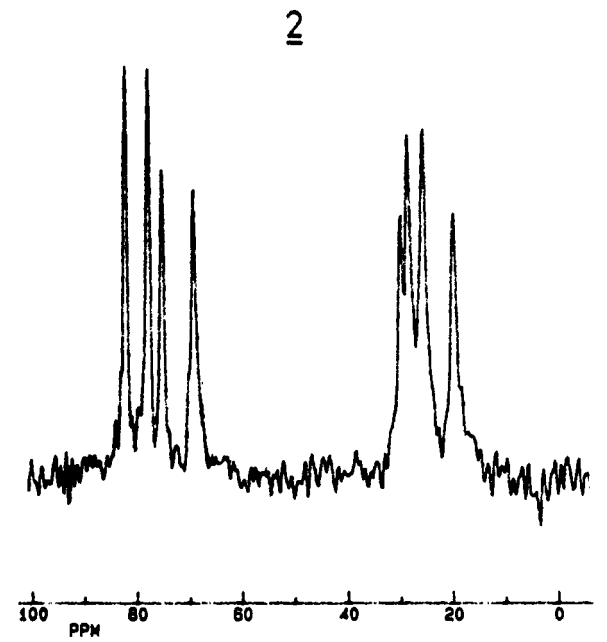

Figure 4. 45.3-MHz solid-phase ^{13}C NMR spectrum of 2.

The solid-phase ^{13}C spectrum (Figure 3), however, shows eight resonances for 1. This is indicative of a conformationally anchored geometry in the crystal and is consistent with the presence of a true molecular center of symmetry as determined by the original X-ray results[8] or the more refined structure.[9] Although there are substantial chemical shift differences in the solid for each of the eight carbons which are averaged to four environments in solution, the largest difference (7.3 ppm) is found for the aromatic carbons which are ortho to the oxygen i.e. C3 vs C6. The X-ray data [8,9] indicate a torsional angle of ca. 62° for the C3–C2–O2–C7 network, while the value for the C6–C1–O1′–C8′ network is ca. 25°. On the basis of the experimental[16] and theoretical[17] angular dependence of the steric shift in ^{13}C NMR we tentatively assign the more shielded resonance to C6. It is interesting to note that the effect is considerably attenuated at the aliphatic carbons C7 vs C8, since the difference at these sites is only 2.8 ppm. It is possible that there is an additional electronic effect

(14) Anet, F. A. L.; Krane, J.; Dale, J.; Daasvatn, K.; Kritiansen, P. O. *Acta Chem. Scand.* **1973**, *27*, 3395.
(15) Borgen, G.; Dale, J.; Daasvatn, K.; Krane, J. *Acta Chem. Scand. B* **1980**, *34*, 249.
(16) Wilson, N. K.; Stothers, J. B. *Top. Stereochem.* **1973**, *8*, 1.
(17) Seidman, K.; Maciel, G. E. *J. Am. Chem. Soc.* **1977**, *99*, 659.

Table I. Bond Lengths (Å) and Angles (deg) Involving Non-H Atoms Only

2

O1–C1	1.4269 (20)	C2–C3	1.520 (3)
O1–C8′	1.416 (3)	C3–C4	1.508 (4)
O2–C2	1.426 (3)	C4–C5	1.513 (3)
O2–C7	1.415 (3)	C5–C6	1.522 (3)
C1–C2	1.507 (4)	C7–C8	1.485 (3)
C1–C6	1.504 (3)	C8–O1′	1.416 (3)
O1–O1′	3.653 (3)	O2–O2′	4.557 (3)
C1–O1–C8′	113.00 (13)	C1–C2–C3	110.03 (22)
C2–O2–C7	116.69 (19)	C2–C3–C4	111.34 (22)
O1–C1–C2	111.43 (17)	C3–C4–C5	111.74 (22)
O1–C1–C6	110.33 (15)	C4–C5–C6	111.40 (19)
C2–C1–C6	111.52 (18)	C1–C6–C5	110.13 (17)
O2–C2–C1	107.98 (19)	O2–C7–C8	111.83 (17)
O2–C2–C3	109.79 (21)	O1′–C8–C7	110.30 (18)

3

O1–C1	1.422 (7)	C3–C4	1.510 (11)
O1–C8′	1.421 (6)	C4–C5	1.516 (11)
O2–C2	1.440 (7)	C5–C6	1.515 (10)
O2–C7	1.428 (7)	C7–C8	1.515 (10)
O1′–C8	1.417 (7)	C1′–C2′	1.534 (9)
O1′–C1′	1.415 (9)	C1′–C6′	1.500 (8)
O2′–C2′	1.446 (7)	C2′–C3′	1.529 (10)
O2′–C7′	1.431 (7)	C3′–C4′	1.508 (11)
C1–C2	1.529 (8)	C4′–C5′	1.515 (11)
C1–C6	1.515 (9)	C5′–C6′	1.516 (11)
C2–C3	1.523 (9)	C7′–C8′	1.498 (9)
O1–O1′	3.990 (7)	O2–O2′	4.180 (7)
C1–O1–C8′	114.1 (4)	O2–C7–C8	113.4 (6)
C2–O2–C7	114.7 (5)	O1′–C8–C7	110.1 (6)
C8–O1′–C1′	114.7 (5)	O1′–C1′–C2′	113.3 (5)
C2′–O2′–C7′	114.3 (5)	O1′–C1′–C6′	108.1 (5)
O1–C1–C2	112.8 (5)	C2′–C1′–C6′	112.2 (5)
O1–C1–C6	108.2 (5)	O2′–C2′–C1′	106.9 (5)
C2–C1–C6	112.1 (6)	O2′–C2′–C3′	110.4 (6)
O2–C2–C1	106.8 (5)	C1′–C2′–C3′	110.2 (5)
O2–C2–C3	111.3 (6)	C2′–C3′–C4′	111.9 (6)
C1–C2–C3	110.6 (5)	C3′–C4′–C5′	110.1 (7)
C2–C3–C4	112.0 (6)	C4′–C5′–C6′	111.5 (6)
C3–C4–C5	112.1 (7)	C1′–C6′–C5′	112.0 (6)
C4–C5–C6	111.1 (6)	O2′–C7′–C8′	113.7 (5)
C1–C6–C5	111.5 (6)	O1–C8′–C7′	109.8 (5)

3·LiNCS

S–C17	1.626 (5)	C1–C2	1.530 (6)
O1–C1	1.447 (5)	C1–C6	1.495 (7)
O1–C16	1.436 (6)	C2–C3	1.530 (6)
O1–Li	2.086 (8)	C3–C4	1.511 (8)
O2–C2	1.433 (6)	C4–C5	1.524 (8)
O2–C7	1.429 (6)	C5–C6	1.536 (7)
O2–Li	2.149 (8)	C7–C8	1.431 (8)
O3–C8	1.444 (6)	C9–C10	1.496 (6)
O3–C9	1.419 (6)	C9–C14	1.508 (6)
O3–Li	2.050 (7)	C10–C11	1.510 (8)
O4–C10	1.454 (5)	C11—C12	1.526 (9)
O4–C15	1.417 (6)	C12—C13	1.497 (10)
O4–Li	2.136 (8)	C13–C14	1.524 (9)
N–C17	1.148 (6)	C15–C16	1.497 (7)
N–Li	1.969 (8)	O1–O3	3.540 (6)
O2–O4	4.002 (5)		
C1–O1–C16	114.0 (3)	O3–C8–C7	110.0 (4)
C1–O1–Li	110.2 (3)	O3–C9–C10	106.6 (4)
C16–O1–Li	105.7 (3)	O3–C9–C14	113.3 (4)
C2–O2–C7	116.7 (3)	C10–C9–C14	112.2 (4)
C2–O2–Li	111.6 (3)	O4–C10–C9	111.3 (4)
C7–O2–Li	105.6 (3)	O4–C10–C11	106.9 (4)
C8–O3C9	112.2 (4)	C9–C10–C11	112.1 (5)
C8–O3–Li	113.6 (3)	C10–C11–C12	111.1 (6)
C9–O3–Li	115.5 (3)	C11–C12–C13	111.1 (5)
C10–O4–C15	117.2 (4)	C12–C13–C14	111.4 (6)
C10–O4–Li	107.5 (3)	C9–C14C13	111.1 (4)
C15–O4Li	110.2 (3)	O4–C15–C16	111.7 (4)
C17–N–Li	175.3 (5)	O1–C16–C15	106.4 (4)
O1–C1–C2	109.9 (3)	S–C17–N	178.1 (4)
O1–C1–C6	107.8 (4)	O1–Li–O2	79.2 (3)
C2–C1–C6	112.2 (4)	O1–Li–O3	117.8 (3)
O2–C2–C1	105.0 (3)	O1–Li–O4	78.9 (3)
O2–C2–C3	111.8 (4)	O1–Li–N	125.9 (4)
C1–C2–C3	110.4 (4)	O2–Li–O3	79.8 (3)
C2–C3–C4	112.0 (4)	O2–Li–O4	138.1 (4)
C3–C4–C5	111.0 (5)	O2–Li–N	103.8 (4)
C4–C5–C6	110.7 (4)	O3–Li–O4	79.5 (3)
C1–C6–C5	110.4 (4)	O3–Li–N	115.9 (4)
O2–C7–C8	112.8 (5)	O4–Li–N	118.0 (4)

operating at the ortho aromatic carbons C3 and C6 due to the spatial orientation of the oxygen lone pairs relative to the plane of the aromatic ring.

For the C3–C2–O2–C7 network in the solid, one of the lone pairs will lie in the plane of the aromatic ring while the other is ca. 60° out of plane. In the case of the related C6–C1–O1′–C8′ network, one of the oxygen lone pairs is essentially perpendicular to the plane of the ring while the other is ca. 15° out of plane. The optimal geometry for conjugative electron release will be that in which the orbitals on O are perpendicular to the plane of the aromatic ring. Hence the carbons which are ortho and para to O1′ are anticipated to be more shielded than those situated ortho and para to O2. Thus the greater sensitivity of the aromatic carbons to the steric shift can be explained by including the additional influence of electronic effects.

The chemical shift difference (3.9 ppm) between the aromatic carbons C4 and C5 in the solid must reflect electronic rather than steric influences. On the basis of the arguments presented in the previous paragraph, C4 is expected to be more shielded than C5.

(ii) *cis-anti-cis*-Dicyclohexano-12-crown-4 (2). In solution,[18] under low-temperature conditions where ring inversion is slow on the ^{13}C NMR time scale, this molecule has been shown to exist as a mixture of two conformations in the ratio of ca. 3:1. The ^{13}C NMR CPMAS spectrum (Figure 4) of solid **2**, however, suggests the presence of only one conformation in the crystal, since only eight resonances are observed. Furthermore, it appears from the solid-phase spectrum that the asymmetric unit in the crystal is half a molecule since there are only four oxygenated carbon resonances in the range 60–85 ppm and four non-oxygenated resonances in the range 15–30 ppm. This is consistent with the X-ray structural results for **2**, as depicted in Figure 2. The molecule possesses local 2-fold symmetry in the form of a 2-fold rotational axis.

With respect to the ^{13}C chemical shifts in solid **2**, a number of interesting trends exist. The lowest field absorption at 82.0 ppm arises from the C1,1′ methine carbons bearing equatorial oxygen and its position is within ca. 1 ppm of that found for the corresponding carbon of the major conformation of **2** in solution at low temperature.[18] Its counterpart C2,2′ bearing an axial oxygen appears at 77.7 ppm, a finding which is in accord with the well-documented axial vs equatorial effects of oxygen on the directly bonded carbon of a cyclohexane ring.[16] Recently[19] at least part of the difference in ^{13}C chemical shift between

(18) Buchanan, G. W.; Kirby, R. A.; Bourque, K. *Can. J. Chem.* **1989**, *67*, 449.

(19) Whitesell, J. K.; Minton, M. A. *J. Am. Chem. soc.* **1987**, *109*, 225.

Table II. Torsion Angles Involving Ring Skeletal Atoms of 12-Crown-4 Systems[a]

12-crown-4[a]			value		3·LiNCS		12-crown-4·LiNCS	
atoms	value	atoms	2	3	atoms	value	atoms	value
O2-C3-C4-O1′	74.5	O1-C1C2-O2	62.2	55.1	O1-C1-C2-O2	54.3	O1-C1-C2-O2	63
C2-O2-C3-C4	-173.6	C7-O2-C2-C1	-149.4	-155.1	C7-O2-C2-C1	-161.9	C8-O1-C1-C2	-173
C3-O2-C1-O1	102.7	C2-O2-C7-C8	106.1	77.2	C2-O2-C7-C8	80.7	C1-O1-C8-C7	74
O1-C1-C2-O2	-75.4	O2-C7-C8-O1′	-78.2	69.2	O2-C7-C8-O3	46.6	O4-C7-C8-C1	60
C4′-O1-C1-C2	140.2	C7-C8-O1′-C1′	165.4	-170.3	C9-O3-C8-C7	-157.7	C6-O4—C7C8	-173
C3′-C4′-O1-C1	-85.2	C8-O1′-C1′-C2′	-99.1	76.1	C8-O3—C9-C10	166.8	C7-O4—C6-C5	96
O2′-C3′-C4′-O1	-74.5	O1′-C1′-C2′-O2′	-62.2	55.6	O3-C9-C10-O4	-49.2	O3-C5-C6-O4	50
C2′-O2′-C3′-C4′	173.6	C7′-O2′-C2′-C1′	149.4	-152.9	C15-O4-C10-C9	-84.6	C4-O3-C5-C6	-155
C3′-O2′-C1′-O1′	-102.7	C2′-O2′-C7′-C8′	-106.1	75.4	C10-O4-C15-C16	104.1	C5-O3-C4-C3	89
O1′-C1′-C2′-O2′	75.4	O2′-C7′-C8′-O1	78.2	71.4	O4-C15-C16-O1	50.0	O2-C3-C4-O3	46
C4-O1′-C1′-C2′	-140.2	C1-O1-C8′-C7′	-165.4	-171.8	C1-O1-C16-C15	-176.3	C2-O2-C3-C4	-162
C3-C4-O1′-C1′	85.2	C8′-O1-C1-C2	99.1	74.6	C16-O1-C1-C2	76.8	C3-O2-C2—C1	84
		C1-C2-C3-C4	-55.9	-53.7	C1-C2-C3-C4	-53.8		
		C2-C3-C4-C5	54.4	54.8	C2-C3-C4-C5	55.2		
		C3-C4-C5-C6	-54.0	-54.8	C3-C4-C5-C6	-56.3		
		C4-C5-C6-C1	55.3	54.7	C4-C5-C6-C1	57.0		
		C2-C1-C6-C5	-57.9	-55.0	C2-C1-C6-C5	-56.7		
		C6-C1-C2-C3	58.2	54.0	C6-C1-C2-C3	55.0		
		C8′-O1-C1-C6	-136.4	-160.9	C16-O1-C1-C6	-160.6		
		O1—C1-C2-C3	-178.0	176.4	O1-C1-C2-C3	174.9		
		O1C1-C6-C5	177.7	180.0	O1-C1-C6-C5	-177.9		
		C7-O2-C2-C3	90.7	84.1	C7-O2-C2-C3	78.3		
		O2-C2-C3-C4	62.8	64.9	O2-C2-C3-C4	62.7		
		C6-C1-C2-O2	-61.6	-67.3	C6-C1-C2-O2	-65.7		
		C1′-C2′-C3′-C4′	55.9	-55.3	C9-C10-C11-C12	54.2		
		C2′-C3′-C4′-C5′	-54.4	57.4	C10-C11-C12-C13	-55.3		
		C3′-C4′-C5′-C6′	54.0	-56.7	C11-C12-C13-C14	55.8		
		C4′-C5′-C6′-C1′	-55.3	55.2	C12-C13-C14-C9	-55.1		
		C2′-C1′-C6′-C5′	57.9	-53.4	C10-C9—C14-C13	53.8		
		C6′-C1′-C2′-C3′	-58.2	52.9	C14-C9-C10-C11	-54.0		
		C8-O1′-C1′-C6′	136.4	-158.9	C8-O3-C9-C14	-69.4		
		O1′-C1′-C2′-C3′	178.0	175.7	O3-C9-C10-C11	70.5		
		O1′-C1′-C6′-C5′	-177.7	-17..1	O3-C9-C14-C13	-66.9		
		C7′-O2′-C2′-C3′	-90.7	8m.2	C15-O4-C10-C11	152.7		
		O2′-C2′-C3′-C4′	-62.8	62.6	O4-C10-C11-C12	176.5		
		C6′-C1′-C2′-O2′	61.6	-67.1	C14-C9-C10-O4	-173.7		

[a] Estimated standard deviations are: 0.1° for 12-crown-4, 0.1–0.2° for 2, 0.4–0.8° for 3, 0.3–0.7° for 3·LiNCS, 1° for 12-crown-4·LiNCS.

Table III. ^{13}C Chemical Shifts (δ_c from TMS ± 0.1)

carbon	1 (solid)	1 (solution)[e]	2 (solid)	2 (solution)[e]	3 (solid)	3 (solution)[e]	3·LiNCS (solid)	3·LiNCS (solution)
1	(150.6)[a]	150.8	82.0	78.4	7,.4	74.5	79.7	75.8
1′	(150.6)[a]	150.8	82.0	78.4	78.4	74.5		
2	(15i.1)[a]	150.8	77.7	78.4	65.5	74.5	69.7	75.8
2′	(152.1)[a]	150.8	77.7	78.4	65.5	74.5		
3	121.3	119.2	28.5	28.2	26.5	27.6	26.2	27.0
3′	121.3	119.2	28.5	28.2	26.5	27.6		
4	122.8	123.2	19.9	22.5	(19.1)[b]	22.5	1..3	21.8
4′	122.8	123.2	19.9	22.5	(22.1)[b]	22.5		
5	126.7	123.2	25.6	22.5	26.5	22.5	24.2	21.8
5′	126.7	123.2	25.6	22.5	265	22.5		
6	114.0	119.2	29.9	28.2	26.5	27.6	27.5	27.0
6′	114.0	119.2	29.9	28.2	28.8	27.6		
7	75.0	71.0	75.1	70.1	(67.8)[c]	65.8	(66.8)[d]	65.3
7′	75.0	71.0	75.1	70.1	(66.4)[c]	65.8		
8	72.2	71.0	69.1	70.1	(66.6)[c]	65.8	(68.3)[d]	65.3
8′	72.2	71.0	69.1	70.1	(63.9)[c]	65.8		
9							69.7	75.8
10							79.7	75.8
11							27.5	27.0
12							24.2	21.8
13							19.3	21.8
14							26.2	27.0
15							(65.2)[d]	65.3
16							(63.9)[d]	65.3

[a–d] Parentheses denote possible interchange of assignments. [e] 0.1 M in CD_2Cl_2 at 298 K.

carbons bearing axial and equatorial substituents has been suggested to arise from anti vicinal C-H–C-H interactions. According to this approach, each anti vicinal interaction will lead to a deshielding of 3 ppm at carbon. Hence a carbon with a single equatorial substituent would be expected to be deshielded by ca. 3 ppm relative to its counterpart with an axial non-hydrogen functionality. In this instance the difference is 4.3 ppm.

The gauche-γ effect[16] of axial oxygen will cause the resonance for C4,4′ to be shielded relative to that for the

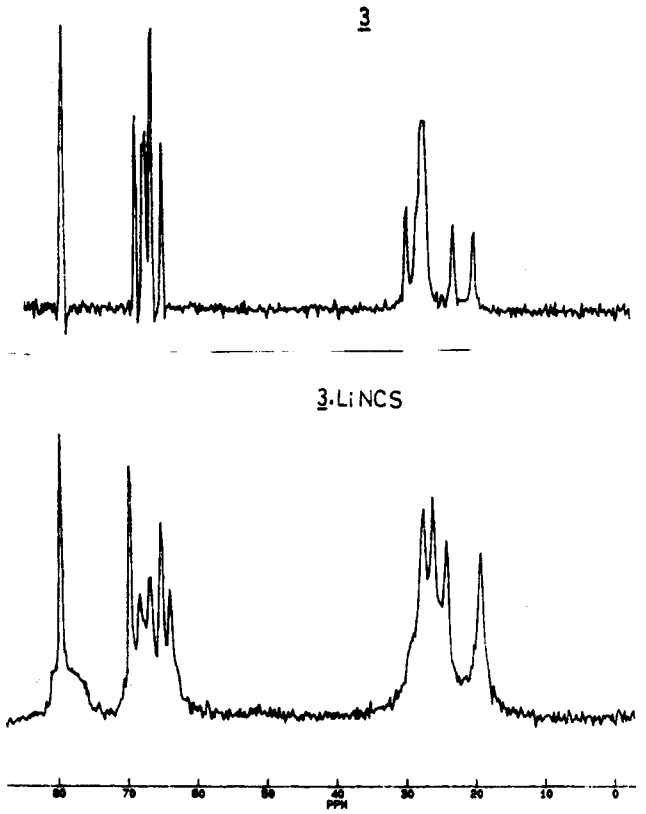

Figure 5. 45.3-MHz solid-phase ^{13}C NMR spectra of **3** and **3**·LiNCS.

corresponding carbons C5,5′ which are located in a trans-γ relationship to the equatorial oxygen atoms. Hence we assign the ∂_C = 19.9 line to C4,4′ and that at ∂ = 25.6 to C5,5′. These chemical shifts are essentially identical with those for the major conformation of **2** in solution at low temperature.

In solution at low temperature,[18] the carbons β to oxygen i.e. C3,6 appear at 28.23 ppm, and no resolution of the resonances for C3 vs C6 is possible even at 198 K. In the solid, there is a resolvable difference between these sites with two resonances appearing at 28.5 and 29.9 ppm. By analogy with related systems in solution,[16] we tentatively attribute the more shielded resonance to C3,3′, which is situated β to the axial oxygen atom. This effect can also be interpreted in terms of the number of anti vicinal C–H interactions.[19]

For the methylene carbons bearing oxygen there is nearly 6 ppm difference in the chemical shifts, with these resonances appearing at 75.1 and 69.1 ppm, respectively. In the crystal structure, each of these carbons is present, either as a terminal or a central atom in five torsional networks. To facilitate comparison, these networks are delineated for C7 and C8 in Chart I. Since both C7 and C8 are present as central atoms in the O–C–C–O fragment with torsional angle of 78.2°, this can be considered as a common unit and thus omitted from the comparison. Detailed examination of the remaining four networks indicates no clear reason for a 6 ppm chemical shift difference between these sites on the basis of torsional angle effects alone.

The suggested importance of anti vicinal C–H interactions in influencing the ^{13}C chemical shifts of the directly bonded carbons[19] has been already been discussed. In the present molecule it is of interest to attempt an analysis using the same concepts but with the consideration of the interactions between *vicinal electron pairs on oxygen and vicinal C–H bonds*. In fact we have a unique opportunity to do so in the present study since the X-ray data and solid-phase chemical shifts are both available.

The key Newman projections here are the C7–C8–O1′–C1′ network which represents the equatorial oxygen linkage to the cyclohexane ring and the corresponding network for the axial oxygen C8–C7–O2–C2. These Newman projections are shown below.

C7–C8–O1′–C1′ C8–C7–O2–C2

In the C7–C8–O1′–C1′ network, the torsional angle between C7 and C1′ is 165.1°, hence the same angles exist between the oxygen lone pairs and the vicinal C–H bonds on C8. Thus there are two transoid interactions present for this network. By contrast, in the C8–C7–O2–C2 network the torsional angle is found to be 106.2°, so that the oxygen lone pairs are nearly eclipsed (θ = 13.8°) with the C7–C8 bond in one case and with the C7–H bond in the other. For the analogous vicinal C-H–C-H interactions it has been found[19] that each anti (or trans) interaction leads to a deshielding of ca. 3 ppm at the directly bonded carbon. If the same magnitude of the effect applies in the oxygenated cases, one would expect to observe the ^{13}C NMR resonance for C7 approximately 6 ppm downfield from that found for C8, in good agreement with that found.

(iii) *cis-syn-cis*-Dicyclohexano-12-crown-4 (3). The single-crystal X-ray determination yielded the structure depicted below for **3**. In this structure, there is a 2-fold rotational axis of symmetry, and hence one anticipates eight unique ^{13}C resonances in the solid-phase NMR spectrum in the absence of any accidental resonance overlap, since the asymmetric unit is half the molecule.

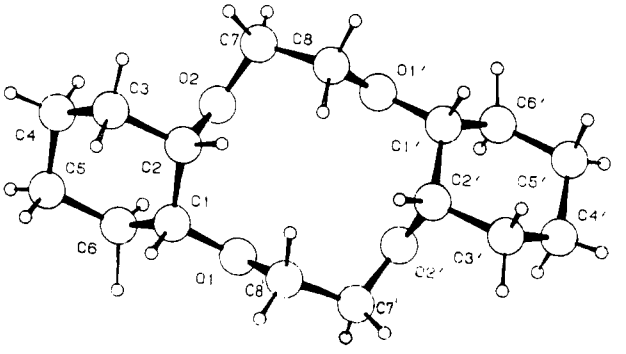

The observed spectrum (Figure 5) is clearly at variance with this expectation, in that a total of ten resonances are resolved, with several more overlapping in the high-intensity absorption near 27 ppm.

There are two possible origins for this apparent nonagreement between the asymmetric unit as identified from the X-ray crystal structure and the ^{13}C CPMAS spectrum. The first is that an atypical crystal may have been selected for the X-ray analysis, so that its structure does not reflect accurately the overall composition of the macroscopic powdered solid used for the NMR spectrum. Secondly, there is the possibility that *intermolecular* crystal packing effects are converting nuclei which are symmetry equivalent from an *intramolecular* standpoint into nuclei which are nonequivalent crystallographically. Such a case has been documented for benzo-15-crown-5 ether,[10] where doubling of resonances in the ^{13}C CPMAS spectrum was observed and attributed to this phenomenon.

To check for the first possibility, an X-ray powder pattern was determined for the same sample of **3** which was employed for the solid-phase NMR spectrum. The results (vide infra) indicate clearly that the symmetry properties of the powdered sample are the same as those for the crystal used in the X-ray analysis. In order to investigate the influence of crystal-packing effects, intermolecular C–C,O distances were obtained from the X-ray data. These data verify that there *is* an intermolecular packing arrangement in **3** which removes the 2-fold symmetry element which is present from consideration of intramolecular geometry only.

This packing arrangement for two molecules is depicted below (ac projection). As a result of this effect and the loss of symmetry, a total of 16 resonances are expected in the ^{13}C CPMAS spectrum of **3** in the absence of any accidental peak overlap. Experimentally, however, only the C7,7′ and C8,8′ pairs are resolved, leading to the total of 10 observed resonances.

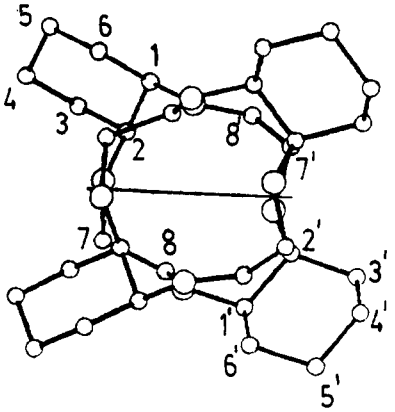

There is accidental overlap in the methine region where only two resonances, at 78.4 and 65.5 ppm, are observed of the four expected. Apparently the crystal-packing effects are not sufficiently strong at the methine carbons to render their shifts inequivalent (vide infra).

The most remarkable feature, however, of the ^{13}C shift data for **3** is the 12.9 ppm difference observed between methine carbons bearing axial and equatorial oxygen. By contrast, the chemical shift difference between the corresponding sites of **2** is only 4.3 ppm. Similar trends have been observed in the solution ^{13}C spectra at temperatures where cyclohexane inversion is slow on the NMR time scale.[18] Furthermore, the shielding difference between isomers is most pronounced at the C2 site, i.e. the carbon which bears axial oxygen. For **2**, this resonance occurs at 77.7 ppm in the solid-phase spectrum, while in **3** it appears at 65.5 ppm. Another point to note here is the fact that the C1 position (i.e. carbon bearing equatorial oxygen) of **3** is shielded by 3.6 ppm relative to C1 of **2**.

Examination of the X-ray data for **2** and **3** reveals an important difference in the dihedral angle for the O–C1–C2–O torsional networks. For **2** this angle is 62.5°, while in **3** it has contracted substantially to 55.5°. This contraction of the torsional angle will tend to shield both C1 and C2 of **3** relative to the corresponding sites of **2**, based on the established angular dependence of the γ-steric shift.[16,17]

Similarly, there is a cyclohexane ring flattening in **3** relative to **2** which will cause an additional shielding for C1 and C2 of **3**. This is apparent in the values observed for the C1–C2–C3–C4 network (53.4° in **3** vs 55.3° in **2**) and the C6–C1–C2–C3 network (53.3° in **3** vs 58.0° in **2**).

There are also several contributing factors in the structure of **3** which will tend to increase the shielding at C2 relative to the corresponding carbon **2**. Examination of the torsional angles for these carbons reveals several interesting differences in their environments relative to the crown ether portions of these molecules. For example, in **3**, the torsional angle for the network C2–O2–C7–C8 is 76.9°, while that for the corresponding network in **2** is 106.2°. This large difference will tend to strongly shield C2 of **3** relative to C2 of **2** again on the basis of the well-known dihedral angle dependence of the γ-steric shift.[16] Finally it should be noted that the intermolecular crystal packing effects do not play a dominant role in determining the magnitude of the ^{13}C CPMAS shifts observed, since the shifts in solution at low temperature are within 2 ppm of those found in the solid for all carbon sites.

In the case of **3**·LiNCS, the X-ray structure shows that inversion of one of the cyclohexane rings has taken place as depicted below. Hence a type of "molecular recognition" has occurred which permits the oxygen atoms of the crown ether to approach a nearly planar geometry that is required for Li complexation.[20]

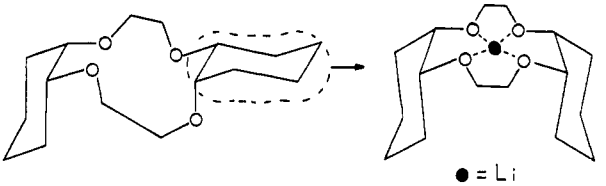

In the crystal structure there is some deviation from a 2-fold symmetry element, especially in the macrocyclic portion of the molecule. The ^{13}C CPMAS spectrum (Figure 5) reflects this, in that there are four resolved CH_2O resonances. The environments of the cyclohexyl carbons of the two rings are not sufficiently different, however, to give rise to two sets of signals. Hence only four nonoxygenated carbon resonances and two CHO carbons are resolved in addition to the aforementioned CH_2O absorptions.

With respect to the four CH_2O resonances, the chemical shifts cover a total range of only 4.4 ppm (i.e. 63.9, 65.2, 66.8, and 68.3). Each of these carbons is involved in eight torsional networks (ignoring hydrogens) so that an attempt to make a clear distinction between them is dangerous at present, since only small differences in dihedral angles are present in many instances.

It is interesting to note that the major difference in the ^{13}C solid-phase shifts between **3** and its LiNCS complex is the 4.2 ppm downfield shift at C2 (the methine carbon bearing axial oxygen) in the complex. Of course, the presence of the Li^+ and the NCS^- perturb the electronic environment so that detailed analysis of factors influencing the shift differences is not warranted.

(iv) Structure of the Cis-Anti-Cis (2) and Cis-Syn-Cis (3) Isomers of Diclohexane-12-crown-4 Ether and the LiNCS Complex of *cis*-*syn*-*cis*-Diclohexano-12-crown-4 Ether (3·LiNCS). ORTEP stereodrawings of **2**, **3**, and **3**·LiNCS with numbering scheme are shown in Figure 2. **2** has a crystallographic center while **3** displays 2-fold symmetry at the molecular level. The direction cosines of the 2-fold axis in the molecule of the asymmetric unit are −0.894 (9), 0.076 (22), 0.440 (18). In **3**·LiNCS,

(20) Buchanan, G. W.; Kirby, R. A.; Ripmeester, J. A.; Ratcliffe, C. I. *Tetrahedron Lett.* **1987**, *28*, 4783.
(21) Le Page, Y. *ACA Meeting Abstr.* **1986**, *14*, 17.
(22) Germain, G.; Main, P.; Woolfson, M. M. *Acta Crystallogr.* **1971**, *A27*, 368.
(23) Gabe, E. J.; Le Page, Y.; Charland, J. P.; Lee, F. L.; White, P. S. *J. Appl. Crystallogr.* **1989**, *22*, 384.
(24) *International Tables for X-ray Crystallography*; Kynoch Press: Birmingham, 1974; Vol. 4.

lithium is pentacoordinated to the four ethereal oxygens of the crown ether and to the nitrogen atom of the SCN^- anion. This coordination scheme and geometry were also found in the lithium complexes of dicyclohexano-13- and -14-crown-4 ethers.[13,25] The four oxygens are not coplanar; the mean deviation from the least-squares plane connecting them is 0.15 Å.

Conformation. Table I lists the bond lengths and angles involving non-H atoms of **2**, **3**, and **3**·LiNCS. Table II lists the torsion angles involving non-H atoms of the macrocyclic ring of **2**, **3**, and **3**·LiNCS along with those in 12-crown-4 ether[1] and its LiNCS adduct.[26] As anticipated, **3** has a smaller binding cavity than dicyclohexano-13-crown-4 ether (**4**). Indeed, the O–O diagonal distances in the 13-membered ring of **4**, O1–O1′, 4.2 Å, and O2–O2′, 4.3 Å, have decreased to 4.0 and 4.2 Å in the 12-membered ring of **3**.

At the molecular level, 12-crown-4 ether (**5**) and **2** have C_i symmetry while **3** and **5**·LiNCS have C_2 and C_4 symmetry, respectively. Overall, **3**·LiNCS is not a symmetrical structure. However, moieties in **3**·LiNCS are symmetry-related. A closer look at Table II shows that portions of **3**·LiNCS are approximately 2-fold and mirror-related. Indeed, the ring-inversion process in **3** that occurred upon Li binding makes the two disubstituted cyclohexyl rings mirror-related. On the other hand, the two ethyl bridging groups are retaining their 2-fold symmetry:

cyclohexano portion (mirror-related)

atoms	angle (deg)	atoms	angle (deg)
C16–O1–C1–C2	77	C15–O4–C10–C9	−85
O1–C1–C2–O2	54	O3–C9–C10–O4	−49
C7–O2–C2–C1	−162	C8–O3–C9–C10	167

ethyl bridging group (2-fold related)

atoms	angle (deg)	atoms	angle (deg)
C2–O2–C7–C8	81	C10–O4–C15–C16	104
O2–C7–C8–O3	47	O4–C15–C16–O1	50
C9–O3–C8–C7	−158	C1–O1–C16–C15	−176

Some torsional angles in **3**·LiNCS indicate that there is some strain in its 12-membered ring. For example, the angle value of O3–C9–C10–O4, a torsional network involving a C–C bond of one of the two cyclohexyl rings, is −49.2°, a value which departs noticeably from the usual range of 55–65° found in analogous structures.[13,25] Most of the torsion angles involving atoms of the ethyl side chains show large deviations to ideal gauche or trans torsion angle values.

As in the X-ray structures of Li^+ complexes of dicyclohexano-13-crown-4 ether,[25] there is a major conformational difference between the structure of **3**·LiNCS and that of the LiNCS complex of dicyclohexano-14-crown-4 arising from the relative orientation of LiNCS with respect to the crown ether itself. In the structure of the lithium complex reported in ref 13, the four oxygens were directed toward the *convex* side of the crown ether, with the cyclohexyl rings pointing away from SCN^-, or, with SCN^- coming in the *convex* side.[4] However, as shown in Figure 2, the four ethereal oxygens in **3**·LiNCS are pointing toward the *concave* side of the crown ether, with the cyclohexyl rings and SCN^- side-by-side, or, with the anion coming in the *concave* side.

Molecular and Translational Symmetry in 3. We stated in a previous paragraph that **3** possesses 2-fold symmetry at the molecular level. Based on this observation, one would expect to find a minimum number of resonances on the ^{13}C CPMAS spectrum of **3**, namely, half the number of carbon atoms in the structure. Unexpectedly, the ^{13}C CPMAS NMR spectrum of **3** (see Figure 5) displayed more resonances than expected, based on the previous assumption. There is also severe overlapping of signals at about 27 ppm. This is indicative of asymmetry in the environment of **3** and, therefore, we must shift our attention and look for some conclusive evidence at the translational symmetry or molecular packing level. Indeed, the solid-state ^{13}C NMR spectrum of benzo-15-crown-5 was reported to show also more lines than expected, based on its X-ray structure showing mirror symmetry at the molecular level.[10] The authors concluded that the difference in the magnetic environment of the atoms was due to asymmetry not at the molecular level but from the packing diagram.[10]

First, the direction cosines of the 2-fold imply that this molecular symmetry element is not parallel to any of the three unit cell length parameters, as demonstrated earlier in the ac projection of the packing diagram of **3**. Second, the stacking arrangement along the *a* axis brings further support to this evidence of asymmetry due to packing as it indicates clearly that the ethano bridges are oriented differently with respect to the $O–C_{ring}–C_{ring}–O$ moities of the neighboring molecule. This prompted us to investigate further this peculiar NMR behavior of **3** using the X-ray structural data.

X-ray powder diffraction on the solid-state NMR sample insured us of the homogeneity of this sample as the powder pattern calculated from the crystal structure was very similar to the experimental powder spectrum. Refinement of the lattice cell parameters from the powder data yielded the following cell parameters:

	cell parameters from	
	X-ray powder data	single-crystal data
a	9.958 (6)	9.957 (2)
b	8.421 (5)	8.426 (2)
c	19.106 (12)	19.101 (3)

They agree within standard deviation with the refined cell parameters obtained from the unique crystal (see the supplementary material for more details).

The environment of all of the carbons of **3** was subsequently checked. Intermolecular interatomic distances were calculated using the published[27] values for the van der Waals radii for C, H, and O. The following limiting distances were obtained: C–C distance of 4.0 Å for a CH–CH interaction; a C–H distance of 3.2 Å for a CH–H interaction and a distance of 3.5 Å for the C–O distance in a CH–O interaction. Results were tabulated and can be found in Table VI. In order to compare the overall environment of each carbon atom, a test based on the general formula for an electric field was employed

$$Z/(\text{interatomic distance})^2$$

where Z is the number of electrons of the atom involved in an intermolecular contact. Next, these individual contributions were summed for each atom. Finally, differences between these sums were calculated for each pair of carbons presumed to be related by 2-fold symmetry. Hence these differences will show for each atomic pair a similarity or a dissimilarity in their magnetic environment. The data in Table VII show that C1/C1′, C2/C2′, and C3/C3′ should not exhibit separate resonances, in agreement with the

(25) Buchanan, G. W.; Kirby, R. A.; Charland, J. P. *Can. J. Chem.* **1990**, *68*, 49.
(26) Groth, P. *Acta Chem. Scand.* **1981**, *35*, 463.
(27) Huheey, J. E. *Inorganic Chemistry: Principles of Structure and Reactivity*, 2nd ed.; Harper and Row: New York, 1978.

Table IV. Crystal Data for 2, 3, and 3·LiNCS

parameter	2	3	3·LiNCS
empirical formula	$C_{16}H_{28}O_4$	$C_{16}H_{28}O_4$	$C_{17}H_{28}LiNO_4S$
formula weight	284.39	284.39	349.41
isomer	cis-anti-cis	cis-syn-cis	
dimensions, mm	0.15 × 0.25 × 0.30	0.2 × 0.3 × 0.3	0.3 × 0.3 × 0.4
crystal system	monoclinic	orthorhombic	
space group	$P2_1/a$	$Pca2_1$	$P2_12_12_1$
a, Å	9.6850 (7)	9.957 (2)	8.746 (4)
b, Å	7.7555 (5)	8.426 (2)	13.180 (5)
c, Å	10.492 (1)	19.101 (3)	16. 2960 (9)
β, deg	100.231 (8)		
Z (molecules/cell)	2	4	
cell volume, Å^3	775.5	1602.5	1878.5
accurate cell parameters from:			
no. of reflns	60	32	50
2θ range	30–41	36–42	109–120
D_{calc}, g cm^{-3}	1.218	1.179	1.235
μ, mm^{-1}	0.08	0.08	1.64
λ, Å	0.70930	(Mo Kα_1)	1.54056 (Cu Kα_1)
octants measd	$\pm h,k,l$; h,k,l	h,k,l; $\bar{h},\bar{k},\bar{l}$	
$2\theta_{max}$, degrees	49.9	49.9	119.8
h range	−11 to 11	0–11	0–9
k range	0–8	0–9	0–14
l range	0–12	0–22	0–18
reflns measd	3082	1506	2294
unique reflns	1344	1459	2001
obsvd reflns	943	794	1884
$I_{net}/\sigma(I_{net})$ ratio		2.5	
R_f (sign. reflns)	0.035	0.030	0.040
R_w (sign. reflns)	0.041	0.031	0.038
goodness-of-fit	1.5	1.2	1.4
weighting scheme	$w^{-1} = \sigma^2(F_o) + 0.0003F_o^2$		
no. of parameters	148	293	330
maximum Δ/σ (last cycle)	0.1	0.2	0.2
final D map background, e/Å^3	≤0.12	≤0.13	≤0.3

observed spectrum. On the contrary, the results for the remaining atom pairs indicate tht separate resonances should be observed in the solid state ^{13}C spectrum, with the C4/C4′ pair expected to exhibit the largest spread. These predictions are consistent with our findings although the observation of a broad resonance with an unresolved shoulder centered at 26.5 ppm precludes a detailed analysis of possible shift differences between the C5/C5′ and C6/C6′ pairs.

Lithium Environment. We reported previously that the adjusted diameter of the binding cavity of the cis-syn-cis isomer of dicyclohexyl-14-crown-4 ether, 1.08 Å, was too small to fit Li^+ (effective diameter 1.18–1.52 Å)[28] within the cavity of the crown oxygens.[13] In this case, the Li cation was instead 0.55 Å out of the plane of the coplanar oxygens, leaving its other side open for anion coordination. In 3·LiNCS, the diagonal distances, O2–O4 and O1–O3, of 4.0 and 3.5 Å, respectively, lead to an adjusted cavity diameter of 0.74–1.20 Å, which is nearly identical with that in the Li complexes of benzo-13-crown-4 ether[29] and dicyclohexyl-13-crown-4.[25] Again, these values are small compared to the effective diameter of Li^+ and thus favor, as expected, 5-coordinate Li^+ complexation.

In 3·LiNCS, Li^+ is lying 0.95 Å out of the mean least-squares plane of the four binding oxygens atoms. The out-of-plane displacements found in 3·LiNCS and LiNCS complexes of dicyclohexano-13- (0.78 Å)[25] and -14-crown-4 (0.55 Å)[13] show the following trend: the Li^+ out-of-plane displacement is increasing with a decrease in the size of the binding cavity of the crown ether. There is a linear relationship between the out-of-plane displacement and the number of atoms forming the crown ether:

size of crown ether =
04.96(Li^+ out-of-plane displacement) + 16.71

correlation coefficient = 0.9963

This linear relationship indicates that a 17-membered ring dicyclohexano crown-4 ether would be required to achieve Li^+ binding in a genuine square-planar pyramid geometry without Li^+ displacement from the plane of the four binding O atoms.

Table V. Atomic Parameters x, y, z, and B_{iso}[a]

	x	y	z	B_{iso}
		2		
O1	0.05660 (12)	0.77506 (17)	0.01174 (11)	3.90 (6)
O2	−0.06039 (13)	0.96231 (16)	0.19837 (12)	3.97 (6)
C1	0.10779 (19)	0.7631 (3)	0.14763 (16)	3.47 (9)
C2	0.08664 (19)	0.9296 (3)	0.21569 (18)	3.86 (9)
C3	0.1468 (3)	0.9144 (4)	0.35921 (21)	5.05 (12)
C4	0.0839 (3)	0.7637 (3)	0.41958 (21)	5.37 (13)
C5	0.0995 (3)	0.5972 (3)	0.34828 (20)	5.07 (11)
C6	0.04026 (22)	0.6138 (3)	0.20440 (18)	3.69 (9)
C7	−0.1023 (3)	1.1373 (3)	0.19428 (19)	4.40 (11)
C8	−0.16401 (23)	1.1928 (3)	0.06086 (21)	4.33 (10)
		3		
O1	0.1630 (3)	0.7711 (4)	0.21322	3.75 (17)
O2	0.2704 (4)	0.9786 (4)	0.3122 (3)	4.00 (17)
O1′	0.2023 (3)	1.2424 (4)	0.2150 (3)	4.14 (18)
O2′	0.0898 (3)	1.0348 (4)	0.1160 (3)	3.79 (16)
C1	0.2582 (6)	0.7185 (7)	0.2636 (3)	3.6 (3)
C2	0.3533 (6)	0.8505 (7)	0.2874 (4)	3.7 (3)
C3	0.4470 (7)	0.7905 (10)	0.3445 (4)	5.1 (3)
C4	0.3709 (9)	0.7168 (10)	0.4047 (4)	5.7 (4)
C5	0.2771 (8)	0.5861 (8)	0.3805 (5)	5.3 (4)
C6	0.1824 (7)	0.6455 (9)	0.3243 (4)	4.7 (3)
C7	0.3319 (8)	1.1316 (7)	0.3092 (4)	4.6 (3)
C8	0.3343 (7)	1.2021 (8)	0.2363 (4)	4.3 (3)
C1′	0.1901 (6)	1.2853 (7)	0.1437 (4)	4.0 (3)
C2′	0.1943 (7)	1.1428 (7)	0.0938 (4)	3.8 (3)
C3′	0.1699 (8)	1.1971 (10)	0.0185 (4)	5.2 (3)
C4′	0.0402 (8)	1.2881 (9)	0.0114 (4)	5.4 (4)
C5′	0.0409 (10)	1.4301 (9)	0.0601 (4)	5.3 (4)
C6′	0.0639 (6)	1.3807 (7)	0.1354 (4)	4.1 (3)
C7′	0.1148 (6)	0.8720 (7)	0.0991 (4)	3.9 (3)
C8′	0.2173 (6)	0.7947 (7)	0.1452 (3)	3.6 (3)
		3·LiNCS		
S	0.04674 (13)	0.21704 (9)	0.29237 (8)	5.35 (6)
O1	0.6308 (3)	−0.02321 (19)	0.37509 (16)	4.25 (13)
O2	0.3702 (4)	−0.13295 (21)	0.37752 (17)	4.69 (14)
O3	0.4277 (3)	−0.14577 (20)	0.21543 (16)	4.67 (13)
O4	0.6430 (3)	−0.00129 (18)	0.21160 (17)	4.29 (13)
N	0.2848 (5)	0.0782 (3)	0.2862 (3)	5.58 (20)
C1	0.5842 (6)	−0.0731 (3)	0.4501 (3)	4.25 (21)
C2	0.4906 (6)	−0.1680 (3)	0.4299 (3)	4.10 (22)
C3	0.4285 (7)	−0.2162 (4)	0.5085 (3)	5.1 (3)
C4	0.3402 (8)	−0.1409 (5)	0.5600 (3)	5.6 (3)
C5	0.4372 (8)	−0.0479 (4)	0.5793 (3)	5.5 (3)
C6	0.4954 (6)	0.0017 (4)	0.5000 (3)	4.42 (23)
C7	0.2928 (7)	−0.2081 (4)	0.3299 (3)	6.8 (3)
C8	0.3750 (8)	−0.2358 (4)	0.2573 (3)	7.2 (3)
C9	0.5539 (6)	−0.1658 (3)	0.1632 (3)	4.10 (22)
C10	0.6195 (6)	−0.0651 (4)	0.1399 (3)	4.35 (21)
C11	0.5160 (9)	−0.0072 (5)	0.0824 (4)	6.1 (3)
C12	0.4761 (10)	−0.0708 (6)	0.0071 (4)	7.5 (4)
C13	0.4074 (8)	−0.1703 (5)	0.0315 (4)	6.2 (3)
C14	0.5126 (7)	−0.2288 (4)	0.0892 (3)	5.1 (3)
C15	0.7811 (5)	−0.0146 (4)	0.2558 (3)	4.61 (24)
C16	0.7561 (6)	−0.0720 (4)	0.3339 (3)	4.94 (24)
C17	0.1846 (5)	0.1344 (3)	0.2886 (3)	3.98 (19)
Li	0.4511 (8)	−0.0223 (5)	0.2909 (5)	4.2 (3)

[a] B_{iso} is the mean of the principal axes of the thermal ellipsoid esds, refer to the last digit printed.

(28) Shannon, R. D. *Acta Crystallogr.* **1976**, *A32*, 751.
(29) Shohan, G.; Lipscomb, W. N.; Olsher, U. *J. Am. Chem. Soc.* **1983**, *105*, 1247.

Table VI. Intermolecular Distances in 3[a]

atom 1	atom 2	inten dist	dist esd	x^2	y^2	z^2	S	L	$Z/(\text{inter dist})^2$	sum of $[Z/(\text{inter dist})^2]$
				C1 at 0.25824, 0.71852, 0.26356						
C1	H6′A	3.112	0.052	0.486	0.688	0.153	3	0 0 0	0.103	0.10
				C4 at 0.37089, 0.71684, 0.40467						
C4	C5′	3.927	0.010	0.459	0.430	0.560	2	0 0 0	0.389	
C4	C7′	3.940	0.010	0.385	0.872	0.599	2	0 0 0	0.387	
C4	H7′B	3.010	0.052	0.361	0.857	0.550	2	0 0 0	0.110	0.89
				C5 at 0.27708, 0.58614, 0.38053						
C5	C4′	3.98	0.01	0.460	0.288	0.511	2	0 0 0	0.378	0.38
				C6 at 0.18236, 0.64553, 0.32429						
C6	C7	3.973	0.010	−0.168	0.868	0.309	3	−1 0 0	0.38	
				C7 at 0.33193, 1.13163, 0.30924						
C7	C3	3.946	0.011	−0.053	1.210	0.345	3	−1 1 0	0.385	
C7	C6	3.973	0.010	0.682	1.354	0.324	3	0 1 0	0.380	0.77
				C8 at 0.33430, 1.20206, 0.23629						
C8	O1	3.310	0.008	0.663	1.229	0.213	3	0 1 0	0.730	
C8	C7′	3.880	0.011	0.615	1.128	0.099	3	0 1 0	0.399	1.13
				C5′ at 0.04085, 1.43013, 0.06009						
C5′	C4	3.927	0.010	0.129	1.717	−0.095	2	0 1 −1	0.389	
C5′	C7′	3.868	0.010	0.115	1.872	0.099	1	0 1 0	0.401	
C5′	C8′	3.895	0.010	0.217	1.795	0.145	1	0 1 0	0.396	1.19
				C6′ at 0.06394, 1.38072, 0.13543						
C6′	C8′	3.813	0.009	0.217	1.795	0.145	1	0 1 0	0.413	
C6′	C8′	3.759	0.009	−0.283	1.205	0.145	3	−1 1 0	0.425	0.84
				C7′ at 0.11478, 0.87199, 0.09910						
C7′	C4	3.940	0.010	0.129	0.717	−0.095	2	0 0 −1	0.387	
C7′	C8	3.880	0.011	−0.166	0.798	0.236	3	−1 0 0	0.399	
C7′	C5′	3.868	0.010	0.041	0.430	0.060	1	0 0 0	0.401	
C7′	H8A	3.057	0.048	−0.124	0.880	0.199	3	−1 0 0	0.107	1.29
				C8′ at 0.21733, 0.79473, 0.14522						
C8′	C5′	3.895	0.010	0.041	0.430	0.060	1	0 0 0	0.396	
C8′	C6′	3.813	0.009	0.064	0.381	0.135	1	0 0 0	0.413	
C8′	C6′	3.759	0.009	0.564	0.619	0.135	3	0 0 0	0.425	
C8′	H6′A	2.828	0.050	0.486	0.688	0.153	3	0 0 0	0.125	1.36

[a] The equivalent positions are (1) x, y, z; (2) $^1/_2 - x, y, ^1/_2 + z$; (3) $^1/_2 + x, -y, z$; (4) $-x, -y, ^1/_2 + z$. The coordinates of bonded atoms are printed on each bond output line. They are derived from the input values with the codes at the end of the line. These codes are *S* and *L*. They are used as follows: 1. Under *S* is the number of the equivalent position used. Apply it to the input x, y, z and renormalize the results to lie between 0 and 1. 2. Under cell are the unit-cell shifts. Apply them.

Table VII. Difference between Sums of $[Z/(\text{inter dist})^2]$ (y) for Carbon Atom Pairs in 3

atom pair	y	atom pair	y
C1, C1′	0.10	C5, C5′	0.81
C2, C2′	0	C6, C6′	0.46
C3, C3′	0	C7, C7′	0.53
C4, C4′	0.89	C8, C8′	0.23

The Li-O_{crown} distances listed in Table I show the following trend: the long and short Li–O bonds are opposite one another unlike the structures described previously.[13,25] The Li–O_{crown} bond lengths range from 2.050 to 2.149 Å. They average 2.11 Å, which is the longest average Li–O bond length reported so far. The average Li–O_{crown} distance in 5·LiNCS is 2.08 Å.[26] This is evidence for the stronger binding of Li^+ by 12-crown-4 than by the more strained dicyclohexano-12-crown-4. The coordination geometry around Li is a distorted square pyramid with Li^+ sitting more or less in the middle of the cavity with the SCN^- ion lying over the Li–O2 bond of the molecule.

Experimental Section

Crystallographic Measurements and Structure Solution and Refinement. Single crystals of **2**, **3**, and **3**·LiNCS were hand-picked, mounted on glass fibers, and measured on a Nonius CAD-4 automatic diffractometer. Accurate cell parameters and intensity data were obtained at room temperature using graphite-monochromated Mo Kα radiation for **2** and **3**, and Cu Kα for **3**·LiNCS. Crystal data are provided in Table IV.

The space groups $P2_1/a$ and $P2_12_12_1$ were uniquely defined from the systematic absences noted in the data of **2** and **3**·LiNCS, respectively. The intensity data for **3** revealed systematic absences consistent with two space groups, namely, *Pcam* and $Pca2_1$. The space group $Pca2_1$ was chosen for **3** based on a Z value of four molecules-per-unit cell (Table IV). This selection proved to be to correct as the X-ray structure of **3** was solved and refined successfully in this space group. Inspection of the structure, using the routine MISSYM,[21] ruled out any possibility of describing it in the centrosymmetric space group *Pcam*. The data were corrected in the usual fashion for Lorentz and polarization-ratio factors but not for absorption. Other details pertaining to the data reduction step are listed in Table IV.

The positions of the non-hydrogen atoms in the three structures were determined by direct methods with MULTAN.[22] At this stage, isotropic refinement of all non-hydrogen atoms was carried out by full-matrix least-squares methods. Subsequent difference maps, in each case, revealed the positions of the H atoms. They were included and refined isotropically while non-H atoms were refined anisotropically. The three structures were refined to convergence by full-matrix least-squares methods; $\sum w(|F_o| - |F_c|)^2$ was minimized with $w^{-1} = \sigma^2(F_o) + 0.0003F_o^2$. Details of the structure refinements and final D-maps are given in Table IV.

All computations were performed with the NRCVAX crystal structure package.[23] The scattering curves were from ref 24. The refined coordinates of the non-H atoms for all compounds are listed in Table V. Bond lengths and angles involving non-H atoms are presented in Table I while torsion angles involving ring skeletal atoms of **2**, **3**, and **3**·LiNCS. are given in Table II. Lists of an-

isotropic temperature factors, hydrogen atomic parameters, all bond lengths and angles, all torsion angles, 2-fold axis calculation for **3**, powder spectrum indexation and lattice parameters refinement from powder the diffractogram of **3**, least-squares mean plane calculation in **3**·LiNCS and calculated, observed, and unobserved structure factors for **2**, **3**, and **3**·LiNCS are available as supplementary material.

X-ray Powder Diffraction Analysis and Lattice Parameter Refinement. The X-ray powder spectrum of **3** was measured to check that the loose crystalline powder of **3** was homogeneous and shared the same crystal structure as found in the hand-picked single crystal. The crystalline powder sample of **3** used for ^{13}C CPMAS solid-state NMR was given additional grinding with a mortar and pestle to get a finer powder for the X-ray powder diffraction experiment. The finely ground powder was loaded in the cavity of a sample holder. The flat blade of a spatula and a glass slide were used to compress gently but firmly the powder and to slice off surplus powder. A new loose layer of powder was deposited and the previous steps repeated.

The sample was measured on a Rigaku D/max-B automated XRD instrument operating in the θ:θ geometry. Diffraction data were obtained using Cu Kα radiation ($\lambda(K\bar{\alpha})$ = 1.541 78 Å). The diffractometer was equipped with a diffracted beam monochromator, a scintillation detector and solid-state counting electronics. The following slit arrangement was used for data collection: divergent slits, 1°; receiving slits, 0.15°; and Soller slits, 1°. The spectral range 5° to 75° (2θ) was measured at 2°/min. The diffractogram of **3** was smoothed and positions of the peak maxima were obtained using manual and computerized searches.

Materials. Synthetic details for the preparation of these systems have been reported elsewhere.[18]

^{13}C CPMAS Spectra. All spectra were recorded at 45.3 MHz using a Bruker CXP-180 NMR instrument via methods described earlier.[13,20]

Acknowledgment. We thank Dr. John Tse of the Chemistry Division of NRC for use of his XRD instrument and preliminary processing of the raw powder diffraction data. G.W.B. thanks the Natural Sciences and Engineering Research Council of Canada (NSERC) for continued financial support via an operating grant. R.A.K. acknowledges the receipt of an NSERC Graduate Fellowship.

Supplementary Material Available: X-ray data for **2**, **3**, and **3**·LiSCN (25 pages); table of structure factors (33 pages). Ordering information is given on any current masthead page.

Stereochemistry of Base-Promoted 1,2-Elimination from *exo*-2-Bicyclo[2.2.1]heptyl Tosylate and Choride

Richard A. Bartsch*,[1] and Jong Gun Lee[2]

Department of Chemistry and Biochemistry, Texas Tech University, Lubbock, Texas 79409-1061, and Department of Chemistry, Pusan National University, Pusan 609-735, Korea

Received May 4, 1990

Elimination reactions of *exo*-2-bicyclo[2.2.1]heptyl tosylate and chloride and their exo-3-deuterated analogues are studied in base–solvent systems that induce clean bimolecular 1,2-eliminations. The relative propensities for competitive syn-exo and anti-endo-H elimination modes are assessed from nonkinetically determined deuterium isotope effects and the deuterium content in the bicyclo[2.2.1]hept-2-ene formed from the deuterated substrates. The competitition between syn-exo and anti-endo-H elimination is influenced by base association, which stabilizes the syn elimination transition state. Potential steric hindrance by oversized dissociated bases has no effect on the elimination stereochemistry.

Introduction

Due to the rigidity of the bicyclo[2.2.1]heptane ring system, studies of base-promoted 1,2-eliminations from 2-monosubstituted and 2,3-disubstituted norbornanes have provided fundamental information concerning the stereochemistry of bimolecular elimination reactions.[3,4] For base-promoted eliminations from exo-2-substituted bicyclo[2.2.1]heptanes, two reaction stereochemistries are possible. Attack of the base on the 3-exo hydrogen as shown in **1** gives syn-exo elimination. Alternatively, base attack on the 3-endo hydrogen as depicted in **2** produces anti-endo-H elimination in which the dihedral angle between the β-hydrogen and the leaving group is much smaller than the optimal dihedral angle of 180° for anti elimination.[5]

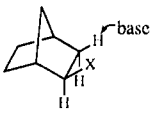

1
(syn-exo)

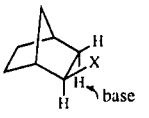

2
(anti-endo-H)

Specific incorporation of deuterium at either the 3-exo or 3-endo position allows these two elimination modes to be differentiated. When Kwart, Takeshita, and Nyce[6] reacted *endo*-3-deuterio-*exo*-2-bicyclo[2.2.1]heptyl tosylate with potassium 3-methyl-3-pentoxide in *p*-cymene at 130 °C, a ratio of 2-deuteriobicyclo[2.2.1]hept-2-ene to bicyclo[2.2.1]-hept-2-ene of 2.2 was obtained. Thus some preference for the syn-exo pathway **1** over anti-endo-H elimination **2** was observed. In a later study conducted by Brown and Liu,[7] the ratio of syn-exo/anti-endo-H

(1) Texas Tech University.
(2) Pusan National University.
(3) LeBel, N. A. *Advances in Alicyclic Chemistry*, Vol 3; Hart, H., Karabatsos, G. T., Eds.; Academic Press: New York, 1971; pp 278–290.
(4) Saunders, W. H., Jr.; Cockerill, A. F. *Mechanisms of Elimination Reactions*; Wiley-Interscience: New York, 1973; pp 79–81.
(5) DePuy, C. H., Bishop, C. A. *J. Am. Chem. Soc.* **1960**, *82*, 2535.
(6) Kwart, H.; Takeshita, T.; Nyce, J. L. *J. Am. Chem. Soc.* **1964**, *86*, 2606.
(7) Brown, H. C.; Liu, K.-T. *J. Am. Chem. Soc.* **1970**, *92*, 200.

0022-3263/91/1956-0212$02.50/0